Received July 13, 2020, accepted July 29, 2020, date of publication August 24, 2020, date of current version September 2, 2020.

Digital Object Identifier 10.1109/ACCESS.2020.3017949

IGBT Remaining Useful Life Prediction Based on Particle Filter With Fusing Precursor

ZHEN RAO, MENG HUANG, (Member, IEEE), AND XIAOMING ZHA, (Member, IEEE)
School of Electrical Engineering and Automation, Wuhan University, Wuhan 430072, China

Corresponding author: Meng Huang (meng.huang@whu.edu.cn)

This work was supported by the National Key Research and Development Program of China under Grant 2018YFB0905705.

ABSTRACT The remaining useful life (RUL) prediction is essential for the IGBT module when setting a reasonable maintenance schedule and improving IGBT reliability by design. In this article, an RUL prediction method is proposed based on the particle filter (P.F.) algorithm with a multi-parameter precursor developed from the IGBT aging data. By fusing the junction temperature (T_j) and collector-emitter on-voltage($V_{CE(on)}$), a new fault precursor is established to monitor IGBTs' condition. A simplified aging model of the precursor is also developed based on a two-stage fitting. After input the historical aging data of the selected IGBT module, the RUL of IGBT can be predicted by the proposed fault precursor based on P.F. algorithm. According to the aging data collected from accelerated aging experiments, the performance of RUL prediction using the fusing precursor is superior to those with the single parameter precursor.

INDEX TERMS IGBT, condition monitoring, RUL prediction, reliability.

I. INTRODUCTION

IGBT module is one of the core devices of the power converter and the second most vulnerable component in the motor drive system [1]–[3]. As listed in the fault distribution report on a CRH3 trains (Wuhan-Guangzhou high-speed railway, from 2009 to 2013) [4], the IGBT failure account for around 64% among all the power converter faults.

To improve the reliability of IGBT, the condition monitoring (CM) technology is widely used to detect early faults of the IGBTs. However, since the health condition of IGBT might degrade to failure within a short time, CM alone is hard to predict the sudden occurrence of catastrophic failure of the device. For the system maintenance, it is more critical to predict the RUL of the IGBTs based on the CM data. The operators of power converters will benefit from the RUL prediction since it helps to make optimized maintenance scheduling and repair plans in a timely manner, especially in high-power applications like high-speed railway systems or high voltage D.C. transmission systems [5].

Much research effort has been carried out to acquire an accurate RUL estimation for IGBTs. The main methods include the model-based method and the data-driven method. As for the model-based prediction method, the industry constructs an analytical model by statistically summarizing a large number of experimental power data like *Coffin-Manson, Norris-Landzberg* [6], *et al.* However, if the material or technology applied to manufacture the device changes, the analytical model parameters need to be re-determined. Consequently, many researchers established physical failure models based on analyzing the stress, strain, energy density, and other mechanical properties of the solder layer during the degradation process [7], in which the aging process such as creep crack expansion is described more accurately. However, there are complex layers and bonding connections in the IGBT structure. It is hard to describe the IGBT internal degradation mechanism in a mathematical way.

The data-driven method could be a more efficient way since we can describe the aging process by some critical precursors of the IGBT and avoiding complex physical modeling. A general data-driven IGBT RUL prediction process can be shown in Fig.1 [8]. Firstly, the accelerated aging experiments are used to speed up the aging and failure of IGBTs. Then, based on data collected in the test, the IGBT prognostic algorithm is developed.

Ahsan *et al.* [9], proposed a data-driven prediction method based on a neural network (N.N.) and an adaptive neuro-fuzzy inference system (ANFIS) model for the degradation of IGBT devices. By comparing the prediction results of RUL of neural network and ANFIS, it shows that the prediction based on the neural network has better performance than that based on ANFIS. Samie *et al.* [10] developed a prediction model

The associate editor coordinating the review of this manuscript and approving it for publication was Yongquan Sun.

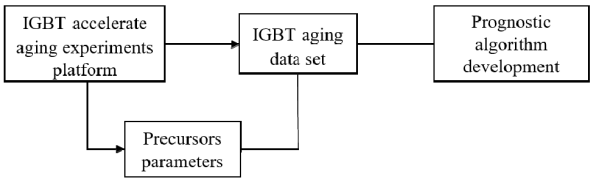

FIGURE 1. A general process for the IGBT RUL prediction [8].

based on fuzzy knowledge and fuzzy system with $V_{CE(on)}$ and ΔV_{CE} as the CM precursors. The experimental data shows that the $V_{CE(on)}$ is the best degradation indicator, and the change of ΔV_{CE} reflects the dynamic process of IGBT degradation [11]. Haque *et al.* [12] put forward a kind of robust estimation method based on auxiliary particle filtering (APF). The method fully reduces the estimated variance by increasing the dimensions and keep the diversity of the samples. In addition, the author employed the APF when IGBT entered the degradation region identified by a simple slope-based method, which can effectively reduce the amount of calculation.

Among the data-driven RUL prediction method mentioned above, P.F. has strong applicability when the researched object is non-linear electronic system mixed with interference noise that the hidden state of the system can be evaluated from the observed quantity containing noise through the filtering process. In addition, the particle filtering method can estimate the system state recursively by combining the prior probability and the current observation value and can update the recursion relation constantly. Therefore, the results can be used for dynamic estimation of RUL and fault diagnosis of IGBT in real-time.

At present, most of the RUL predictions based on P.F. for IGBT are monitoring the IGBT with a single faulty precursor while ignoring the influence of the junction temperature T_j. However, choosing a suitable precursor will play an essential role in IGBT condition monitoring. Some widely adopted precursors include the collector-emitter saturation voltage $V_{CE(on)}$, gate threshold voltage $V_{GE(th)}$, cut-off times T_{off}, case-junction thermal resistance R_{th} [13]–[15]. Research shows that the $V_{CE(on)}$ has a significant sensitivity for the bond-wire lifting off and solder layer fatigue. It is also accurate and able to be on-line measured in a wide temperature range.

Therefore, in this article, a new IGBT failure precursor is proposed by fusing the $V_{CE(on)}$ and T_j to improve the prediction accuracy. Meanwhile, the IGBT wire bond liftoff mechanism is considered in the data-driven modeling method. Furthermore, a new IGBT RUL prediction procedure is proposed based on the particle filter (P.F.). It is verified by the experiment that the P.F. algorithm based on the new fault precursor performs better than the single fault precursor in IGBT RUL prediction.

II. CONSTRUCTION OF FAULT PRECURSOR

As an indicator of IGBT degradation, the $V_{CE(on)}$ can well describe the aging process of IGBT. However, $V_{CE(on)}$ not only changes with the aging of IGBT but is also affected by junction temperature. That is to say, $V_{CE(on)}$ has a strong coupling relationship with T_j. Meanwhile, it is often difficult to maintain a constant temperature during the accelerated aging test. Therefore, CM and life prediction of IGBT must depend on the changes of $V_{CE(on)}$ and T_j. It can be known from formula (1) that $V_{CE(on)}$ is correlated with T_j, and $V_{CE(on)}$ is also affected by the current I_C. However, further theoretical analysis and simulation experiments are needed to research the coupling relationship between the three ones.

$$V_{CE(ON)} = f(I_c, T_j) \tag{1}$$

A. RELATION BETWEEN $V_{CE(on)}$ AND T_j

According to [16], the saturation voltage of IGBT can be expressed as

$$\begin{aligned} V_{CE(ON)}(T_j, I_{CE}) &= f(T_j, I_C) \\ &= [V_0 - a(T_j - T_{j0})] \\ &\quad + [R_0 + b(T_j - T_{j0})] \times I_{CE} \end{aligned} \tag{2}$$

where $V_{CE(on)}$, T_j, and I_C are the saturation voltage, junction temperature, and current of IGBT module, respectively. V_0 and R_0 are the saturation voltage and equivalent resistance of the IGBT power module at the reference junction temperature T_{j0}, respectively. a and b are the temperature coefficients for V and R, respectively. The value of the second term ''$[R_0 + b(T_j - T_{j0})]$'' is positively correlated with junction temperature T_j. The correlation between $V_{CE(on)}$ and T_j is determined by these two terms collectively. Reference [16] points out that when I_C is equal to the high current $I_{C(h)}$, the second term dominates the influence on the value of $V_{CE(on)}$, and $V_{CE(on)}$ is positively correlated with T_j. Substitute $I_C = I_{C(h)}$ into equation (2), we can ignore the former term in equation (2) and get

$$\begin{cases} V_{CE(on)} = R_0 I_C + b I_C (T_j - T_{j0}) = p_1 \times T_j + p_2 \\ p_1 = b I_C, p_2 = (R_0 - b T_{j0}) \times I_C \\ I_C = I_C(h) \end{cases} \tag{3}$$

However, whether $V_{CE(on)}$ and T_j are linear in the condition of high current needs further simulation research to verify.

In order to verify the above theoretical analysis, simulation is carried out in Saber software. As shown in Fig.2, the simulation circuit adopts the IGBT module based on Hefner physical model from Saber software itself. The junction temperature input interface of this module is connected to a heat source. The value of the heat source controls the junction temperature. the dc power supply is adjusted so that the current I_C is equal to the large current under accelerated aging experiment conditions. The switching on and off of IGBT is controlled by a pulse power source. The parameter scanning tool in Saber was used to simulate the junction temperature from 120°C to 200°C (increased by 10°C), and the corresponding $V_{CE(on)}$ was obtained by simulation.

The voltage between the collector and emitter during two periods is shown in Fig.3. The one that is circled in red is

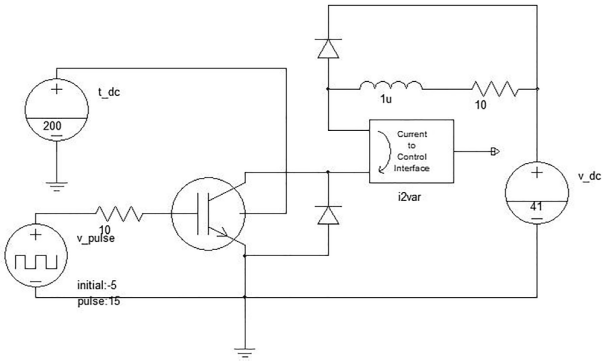

FIGURE 2. Saber simulation circuit under constant current and linearly increasing junction temperature.

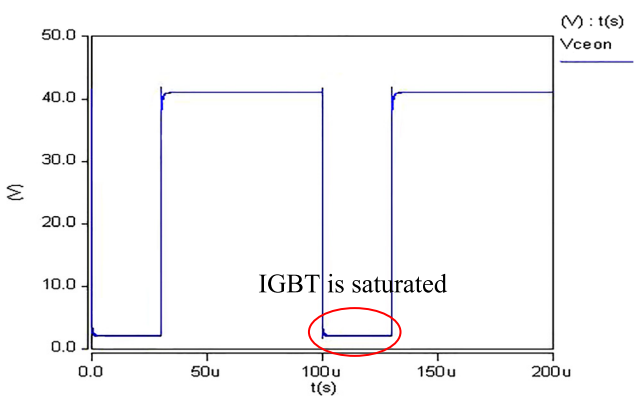

FIGURE 3. Waveform of VCE when IC is certain and Tj varies from 120°C to 200°C.

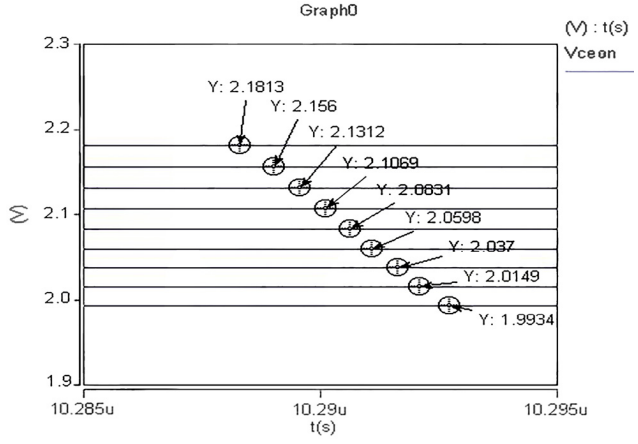

FIGURE 4. Local amplification of waveforms when IGBT is saturated.

when IGBT is saturated, which is shown in Fig.4 after local amplification. As shown in Fig.4, $V_{CE(on)}$ increases approximately linearly when junction temperature varies from 120°C to 200°C at a certain speed.

Record the simulation data and make a scatter diagram $(V_{CE(on)}, T_j)$ of the two-dimensional relationship between $V_{CE(on)}$ and T_j, which approximates a straight line. which shows saturation voltage $V_{CE(on)}$ has a good linear relationship with T_j when I_C remains high current, and the calibration curve of saturation voltage $V_{CE(on)}$ and junction temperature T_j, $V_{CE(on)} = f(T_j)$ can be expressed as follows

$$V_{CE(ON)=p_1 \times T_j + p_2} \tag{4}$$

The value of p1,p2 can be obtained as follows by fitting the scatter diagram $(V_{CE(on)}, T_j)$ acquired from the simulation with the formula (4)

$$p_1 = 0.0003051, \quad p_2 = 1.983 \tag{5}$$

B. PROPOSED PRECURSOR

It's hard for junction temperature kept constant during the accelerated aging experiment. Therefore, in order to eliminate the influence of junction temperature brought on the characteristic precursor $V_{CE(on)}$, which will affect the assessment of IGBT degradation, $V_{CE(on)}$ at different junction temperatures need to be normalized to the same initial junction temperature T_0. Suppose $V'_{CE(on)}$ is the saturation voltage after normalization to T_0.

$$V'_{CE(ON)} = p_1 \times T_0 + p_2 \tag{6}$$

Subtract (6) from (5) and eliminating the common term p_2

$$V'_{CE(ON)} = V_{CE(ON)} - p_1 \times (T_j - T_0) \tag{7}$$

where, $V_{CE(ON)}$ was normalized to equivalent saturated voltage whose junction temperature is at the initial junction temperature T_0 ($T_0 = 120°C$), which is also the definition of the proposed new precursor $V'(V_{CE(on)}, T_j)$ for IGBT condition monitoring as shown in formula (8).

$$V'(V_{CE(ON)}, T_j) = V_{CE(ON)} - p_1 \times (T_j - T_0) \tag{8}$$

The linear relationship of $V_{CE(on)}$ and T_j will be changed along with the degradation of the IGBT module. Relationship between $V_{CE(on)}$ and T_j under different age of IGBT is shown in Fig.5, from which it can be seen that, $V_{CE(on)}$ and T_j remains linear under the same high current I_C. The slope of trend line almost stay the same with the degradation of the IGBT module. That is to say, with the aging process of IGBT, only p_2 changed in formula (4), p_1 remains constant. Therefore, the degradation of IGBT will not affect formula (7), which is exactly the proposed new precursor $V'(V_{CE(on)}, T_j)$.

As IGBT ages, $V_{CE(on)}$ will gradually increases and so does $V'(V_{CE(on)}, T_j)$. When $V'(V_{CE(on)}, T_j)$ is higher than 1.05 times of the initial value V'_0, the IGBT power module can be considered as invalid [13]. Then the failure threshold is

$$V'(V_{CE(ON)}, T_j) = 1.05V'_0 \tag{9}$$

When $V'(V_{CE(on)}, T_j) > 1.05V'_0$, IGBT was judged faulty. Based on the above analysis, the two-dimensional degradation indicator $V'(V_{CE(on)}, T_j)$ including $V_{CE(on)}$ and T_j was determined as the characteristic precursor to monitor IGBT health condition in this article, based on which, P.F. algorithm was used to predict the RUL of IGBT later in the paper.

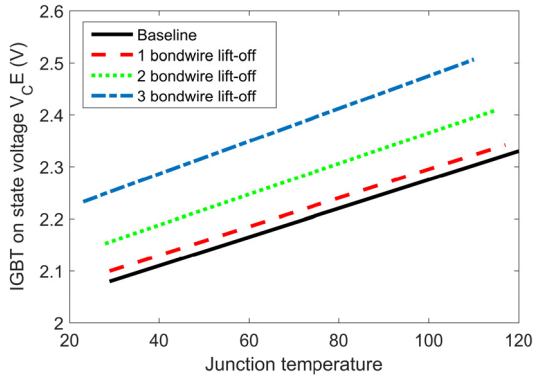

FIGURE 5. Voltage variation with junction temperature at high current[16].

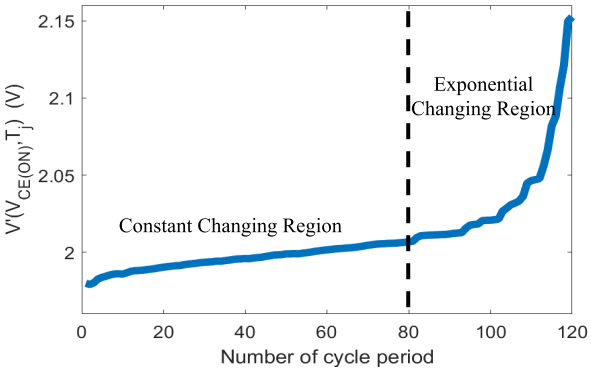

FIGURE 6. The degradation curve of $V'_{CE(ON)}$ after data preprocessing.

III. PARAMETER TRAINING OF DATA DRIVEN MODEL

This part takes the aging data of $V'(V_{CE(on)}, T_j)$ from IGBT sample A as an example to illustrate the establishment of IGBT degradation model and the process of parameters training.

A. PREPROCESS OF THE AGING DATA

Due to the inevitable errors in measurement, there are bad points in the original data. First of all, remove the bad points through rindar criterion [17]. In the meanwhile, the life span of each sample IGBT is different, in other words, the number of the thermal cycles an IGBT experienced from health to failure is different. In order to make the aging model better adjusted to the degradation process of all the IGBT sample, in the paper, the whole life span of each IGBT sample is compressed to 120 cycles before prediction. Assume the number of cycles in the aging experiment is K. Set

$$S = K/120(integer) \tag{10}$$

where S is the number of thermal cycles contained in the compressed period, and set the average value $V'(V_{CE(on)}, T_j)$ of $1\sim S$ period as $V'_1 \sim V'_N$, the aging data after compression is

$$\begin{aligned} V'_{CE(ON),1} &= (V'_1 + V'_2 + \ldots V'_S)/S \\ V'_{CE(ON),2} &= (V'_{S+1} + V'_{S+2} + \ldots V'_{2S})/S \\ &\cdots\cdots \\ V'_{CE(ON),120} &= (V'_{119S+1} + V'_{119S+2} + \ldots V'_{120S})/S \end{aligned} \tag{11}$$

Therefore, one period of the compressed aging data contains N thermal cycle. One cycle of the original data is 6s, so each cycle of $V'_{CE(on)}$ after compression is $6N$s. Plot the degradation curve of $V'_{CE(on),i}$ (i=1∼120) as shown in Fig.6.

B. AGING MODEL SIMPLIFICATION

According to [11], the degradation and resultant change of $V'(V_{CE(on)},T_j)$ can be categorized into three regions. After analyzing the general trend of the aging data obtained from the experimental conditions in the paper, the model is simplified into two regions: constantly changing region and exponential changing region which can be shown as below.

1) CONSTANT CHANGING REGION

Before $V'(V_{CE(on)}, T_j)$ increases its 2% of the initial value, the $V'_{CE(on)}$ increases linearly, which corresponding to the constant change region of IGBT. This region indicates the primary degradation of IGBT, where the upward trend is obvious, but the change in the slope approximates zero. The simplified degradation model can be expressed as follows, which can be used as the health baseline [18].

$$V'_{CE(ON)} = p_1 \cdot n + p_2 \tag{12}$$

where n is the number of the thermal cycle. Equation (12) and Fig.7 obtained from the curve fitting toolbox in MATLAB demonstrate that the first two-thirds of the data has an excellent fitting effect when using line fitting.

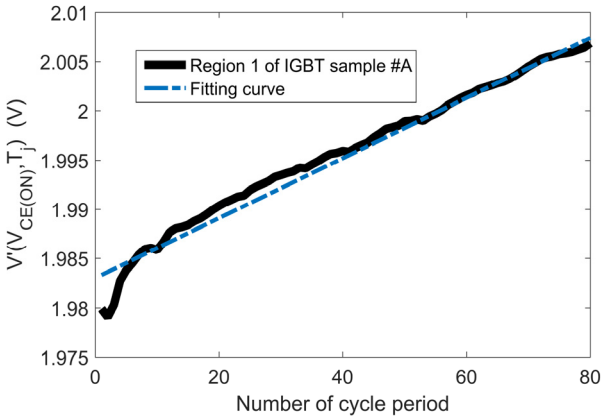

FIGURE 7. Performance of curve fitting for the constant changing region.

2) EXPONENTIAL CHANGING REGION

$V'(V_{CE(on)}, T_j)$ increases exponentially and reaches the threshold value, which indicates the failure of IGBT in this region. The slope of the trend line is significantly changing, and the aging data can be fitted by double exponential function [19], as formula (13) and Fig.8 showed

$$V'_{CE(ON)} = a \cdot \exp(b \cdot n) + c \cdot \exp(d \cdot n) \tag{13}$$

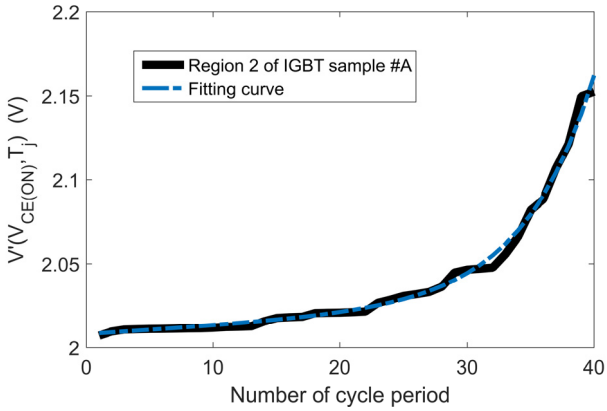

FIGURE 8. performance of curve fitting for the exponential changing region.

C. PARAMETER TRAINING OF THE AGING MODEL

For region 1, the formula (14) obtained from the deformation of equation (12) is applied to train the model parameters, which is also more in line with the form of the P.F. state transition model mentioned in the following contents as page 5 shows.

$$V'_{CE(ON),k} = V'_{CE(ON),k-1} + p_2 + v_{k-1} \tag{14}$$

where p_2 is the slope of the trend line fitted by MATLAB, and v_{k-1} is the process noise.

The expression of $V'_{CE(ON)}$ at kth thermal cycle for formula (13) is as follows

$$V'_{CE(ON),k} = a \cdot \exp(b \cdot k) + c \cdot \exp(d \cdot k) \tag{15}$$

The corresponding model expression at *(k-1)*th cycle is as follows

$$V'_{CE(ON),k-1} = a \cdot \exp(b \cdot (k-1)) + c \cdot \exp(d \cdot (k-1)) \tag{16}$$

The deformed double exponential model is obtained by eliminating the common term $a \cdot \exp(b \cdot k)$ which is expressed as equation (17)

$$V'_{CE(ON),k} = V'_{CE(ON),k-1} \cdot \exp(b) + c \cdot \exp(d \cdot k)(1 - \exp(b - d)) + v_{k-1} \tag{17}$$

The formula (14) and (17) consist of the state transition model required for particle filtering together.

In real working conditions, since the life of IGBT is counted in years, it is difficult to get historical data of the CM parameters that span the whole life period of IGBT. Therefore, the empirical aging model established in this article only uses partial aging data of IGBT. The empirical model of the state transition equation is constructed using 85% (90%, 95% have better performance) of data from sample *A*, which are used to predict the RUL of samples *B, C,* and sample *D,* respectively.

TABLE 1. Results of parameter training of aging model.

Data	p_1	*b*	*c*	*d*
85%A	0.0003051	-0.002385	0.5503	0.00679
90%A	0.0003051	-0.02351	1.839	0.002021
95%A	0.0003051	0.0001122	0.0008541	0.1183

Parameters of the model obtained from fitting sample *A* with the formula (12) and (13) are shown in Table 1. In addition, the curve of original data and the fitting curve with diverse percentage of sample *A* are shown in Fig.9.

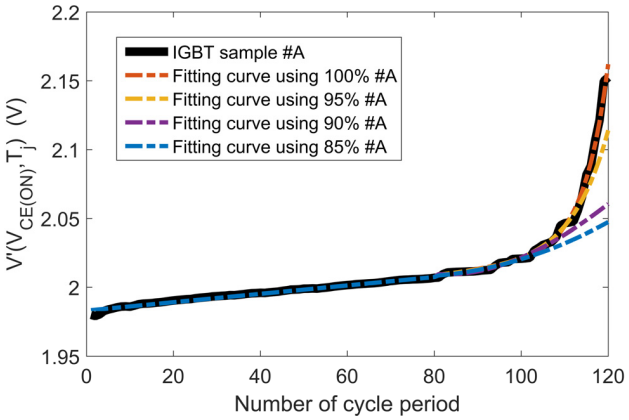

FIGURE 9. The degradation trajectory $V'_{CE(ON)}$ and its fitting curve.

IV. PARTICLE FILTER PREDICTION

Regard one of the sample data as a known sample. The RUL of the target sample is predicted by P.F. algorithm based on the empirical state transition model built from the known sample. Select the first N cycles of the target sample as measured historical value to train the algorithm. When $V'(V_{CE(on)}, T_j)$ reach 1.05 times of its initial value, the target IGBT is considered faulty.

The Input and Output algorithm are as follows:

Input: the first N cycles $V'(V_{CE(on)}, T_j)$ of target sample from experimental data set

Output: RUL estimation and posterior probability density distribution of the target IGBT sample

A. PRINCIPLE OF PARTICLE FILTER ALGORITHM

The Particle filter (P.F.) algorithm is a kind of approximate bayesian filtering algorithm based on the *Monte Carlo* simulation principle, which shows good performance for tracking and predicting the aging of IGBT, a non-linear and non-gaussian complex system.

Firstly, the system model, consisting of state transition model (18) and measurement model (19), needs to be established. At which at least one of the functions, f or h is non-linear [20].

$$V'_{CE(ON),pre,n} = f(V'_{CE(ON),pre,n-1}) + v_{n-1} \tag{18}$$

$$V'_{CE(ON),act,n} = h(V'_{CE(ON),pre,n}) + m_n \tag{19}$$

where the $V'_{CE(ON),pre,k}$ is predicted $V'_{CE(ON)}$ at time k, $V'_{CE-(ON),pre,k}$ is measured $V'(V_{CE(ON)}, T_j)$ at time k, and f, h are respectively the state transition function and measurement function, v and m are process noise and measurement noise respectively, The noise distribution is assumed Gaussian under central limit theorem. Function f is formulated from equation (14) and (17), while function h in the paper is $y{=}x$.

In the Bayesian theory, the problem of state estimation is to calculate the probability density function of the current state recursively utilizing all the previous historical data. It requires two steps of prediction and updates for recursive calculation.

$$\begin{aligned} &p(V'_{CE(ON),pre,1:k-1}|V'_{CE(ON),act,1:k-1}) \\ &= \int p(V'_{CE(ON),pre,k}|V'_{CE(ON),pre,k-1}) \\ &\quad \times p(V'_{CE(ON),pre,k-1}|V'_{CE(ON),act,1:k-1}) dV'_{CE(ON),pre,k-1} \end{aligned} \tag{20}$$

The updating process uses the latest measured value $V'_{CE(ON),act,k}$ to modify the prior probability density to obtain the posterior probability density, as shown in equation (19). The posterior probability here will also be substituted into the next prediction process, forming a recurrence, (21) as shown at the bottom of the next page.

Monte Carlo is a method of approximating the posterior probability density distribution with a set of discrete random sampling points (i.e., a collection of particles). Use the sample mean instead of integral operation to obtain the minimum variance estimate of the state.

However, the specific form of the posterior probability density is not available in an actual system, so it cannot be directly sampled. The Bayes importance sampling method samples from a known and easily sampled reference distribution $q(V'_{CE(ON),pre,k}|V'_{CE(ON),act,1:k})$. As the number of samples increases, the weighted sum approaches the real posterior distribution $p(V'_{CE(ON),pre,k}|V'_{CE(ON),act,1:k})$. Carried out the weighted average of the particles sampled from the reference distribution:

$$\begin{aligned} &E[f(V'_{CE(ON),pre,k})] \\ &= \int f(V'_{CE(ON),pre,k}) \frac{p(V'_{CE(ON),pre,k}|V'_{CE(ON),act,1:k})}{q(V'_{CE(ON),pre,k}|V'_{CE(ON),act,1:k})} \\ &\quad \times q(V'_{CE(ON),pre,k}|V'_{CE(ON),act,1:k}) dV'_{CE(ON),pre,k} \\ &= \frac{1}{N} \sum_{i=1}^{N} f(V'^{(i)}_{CE(ON),pre,k}) w_k^{(i)} \end{aligned} \tag{22}$$

Among which

$$\begin{aligned} w_k^{(i)} &= w_{k-1}^{(i)} \\ &\quad \times \frac{p(V'_{CE(ON),act,k}|V'^{(i)}_{CE(ON),pre,k}) p(V'^{(i)}_{CE(ON),pre,k-1})}{q(V'^{(i)}_{CE(ON),pre,k}|V'^{(i)}_{CE(ON),pre,0:k-1}, V'^{(i)}_{CE(ON),act,1:k})} \end{aligned} \tag{23}$$

Normalize the weights and get $\tilde{w}_k(x_k^{(i)})$, and then substitute it into the formula to get the estimated value of the state at time k.

$$\begin{aligned} &E[f(V'_{CE(ON),act,k})] \\ &\quad = \sum_{i=1}^{N} w_k(V'^{(i)}_{CE(ON),pre,k}) f(V'^{(i)}_{CE(ON),pre,k}) \end{aligned} \tag{24}$$

After many times iterations, the weight of many particles tends to zero [21], which makes a large amount of computation wasted on particles that have little effect on estimating the probability distribution of the posterior filter. That leads to the degradation of estimation performance. What mentioned above is the phenomenon of particle decay. The idea of resampling is to suppress degradation by reproducing a large number of particles with high weights and eliminating the ones with low weights. After resampling, the number of particles remains the same, and the weight of each particle is equal to 1/N. The state estimation formula after resampled is also (24), and the calculation form of the posterior probability density is:

$$\begin{aligned} &p(V'_{CE(ON),pre,k}|V'_{CE(ON),act,1:k}) \\ &\quad = \sum_{i=1}^{N} w_k^{(i)} \delta(V'_{CE(ON),pre,k} - V'^{(i)}_{CE(ON),pre,k}) \end{aligned} \tag{25}$$

B. PREDICTION STEPS

The flow chart of P.F. algorithm is shown in Fig.10.

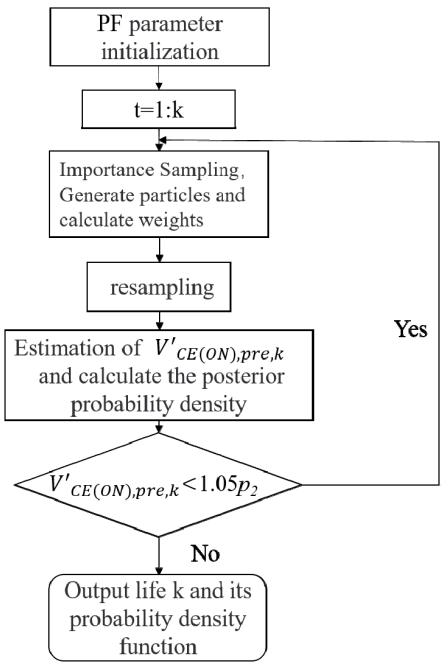

FIGURE 10. Flow chart of P.F. algorithm predicting IGBT RUL.

1) PF PARAMETER INITIALIZATION

Set the number of sampling particles to N. In the initial moment k=0, generate the particle set $\left\{V'^{(i)}_{CE(ON),pre,0}\right\}_{i=1}^{N}$ by

sampling from the prior distribution $p(V'_{CE(ON),pre,0})$, and set the weight value of each particle as $w_0 = 1/N$.

2) IMPORTANCE SAMPLING

For $i=1,\ldots T$, the particle set $\left\{V'^{(i)}_{CE(ON),pre,k}\right\}_{i=1}^{N}$ is generated by sampling from the importance density function $q(V'_{CE(ON),pre,k}|V'_{CE(ON),act,1:k})$. Calculate and normalize the weight of each particle according to equation (23).

3) IMPORTANCE RESAMPLING

Copy and eliminate the particles according to the value of the normalized weight. Extract N particles to form a new set of particles $\left\{V'^{(i)}_{CE(ON),pre,0}\right\}_{i=1}^{N}$, reset the weight to 1/N.

4) RUL ESTIMATION AND ITS PDF CALCULATION

Use formula (24) to calculate the estimated mean value of $V'_{CE(ON),pre,k}$. If it exceeds $1.05p_2$, finish the recursion, in which time the value of k minus the initial prediction cycles equals to the estimated value of the RUL of IGBT. Use equation (25) to calculate the posterior probability density. Determine if the loop is finished. If so, output the result of RUL and its PDF, otherwise return to step 2).

C. ANALYSIS OF THE RESULTS

1) COMPARISON BETWEEN RUL ESTIMATION USING $V'(V_{CE(ON)}, T_J)$ AND $V_{CE(ON)}$ AS CM PRECURSOR

IGBT #B failed at 112 cycle in the experiment. The critical $V_{CE(on)}$ is 5% increasing from mean of initial $V_{CE(on)}$, so does the critical value for $V'(V_{CE(on)}, T_j)$. The. simulated trajectories for different initial prediction cycle are shown for P.F. using $V_{CE(on)}$ as CM precursor and P.F. using $V'(V_{CE(on)}, T_j)$ as CM precursor (Hereinafter referred to as $V_{CE(on)}$ P.F. and $V'(V_{CE(on)}, T_j)$ P.F.)in Fig.11 and Fig.12, respectively. From that, For a 100-initial prediction cycle using $V'(V_{CE(on)}, T_j)$ as CM precursor, the simulated trajectory is sufficiently close to the actual trajectory.

As Fig.11 and Fig.12 shows, when the initial PDF of process noise and measurement noise is N(0, 5e-3) and N(0, 3e-6) respectively. Estimated RUL for $V_{CE(on)}$ P.F. were 63, 73, 84 and 98 when the training cycle was 40, 60, 80 and 100 respectively, while estimated RUL for $V'(V_{CE(on)}, T_j)$ P.F. were 71, 79, 88 and 104 respectively when the training cycle was 40, 60, 80 and 100. It demonstrates that RMS error decreases in line with the increase of initial prediction cycle for both $V_{CE(on)}$ P.F. and $V'(V_{CE(on)}, T_j)$ P.F.

However $V'(V_{CE(on)}, T_j)$ P.F. shows better performance than $V_{CE(on)}$ P.F.As can be seen from the posterior probability density distribution given in Fig.13 or Fig.14, with the increase of training cycle, the peak value of PDF distribution

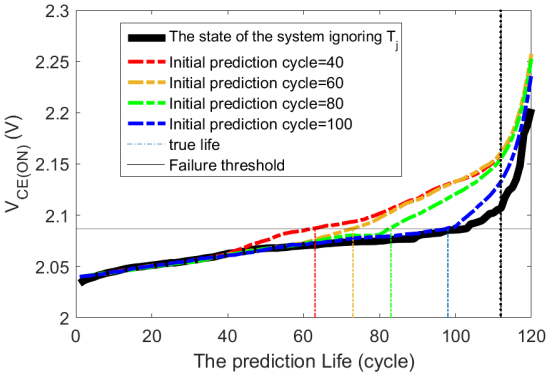

FIGURE 11. RUL prediction results of $V_{CE(on)}$ P.F. under different initial prediction periods.

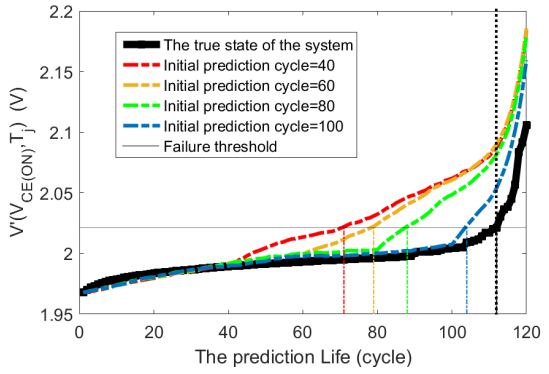

FIGURE 12. RUL prediction results of $V'(V_{CE(on)}, T_j)$ P.F. under different initial prediction periods.

shows a rising trend, and the distribution width on the horizontal axis narrows for both $V_{CE(on)}$ P.F. and $V'(V_{CE(on)}, T_j)$ P.F. It indicates that the longer the training cycle is, the higher the accuracy of the estimated RUL will be, and the closer the peak center will be to the actual life. In addition, comparing Fig.14 with Fig.13, it's observed that peak center of $V'(V_{CE(on)}, T_j)$ P.F. is closer to actual life than that of $V_{CE(on)}$ P.F. under the same initial prediction cycle, which verified the result in Fig.11 and Fig.12. In the meanwhile, the peak value of $V'(V_{CE(on)}, T_j)$ P.F. is more higher than that of $V_{CE(on)}$ P.F. under the same initial prediction cycle which demonstrate that $V'(V_{CE(on)}, T_j)$ P.F. clearly shows improvement in RUL estimation for IGBT than $V_{CE(on)}$ P.F.

2) EFFECT OF NOISE ON $V'(V_{CE(ON)}, T_J)$-PF-BASED RUL ESTIMATION

Particle filtering needs both process noise and measurement noise for its operation. Both state transition equation and measurement equation loss their stochastic nature at the absence of process noise and measurement noise, respectively.

$$p(V'_{CE(ON),pre,k}|V'_{CE(ON),act,1:k}) = \frac{p(V'_{CE(ON),act,k}|V'_{CE(ON),pre,k})p(V'_{CE(ON),pre,k}|V'_{CE(ON),act,1:k-1})}{p(V'_{CE(ON),act,k}|V'_{CE(ON),act,1:k-1})} \quad (21)$$

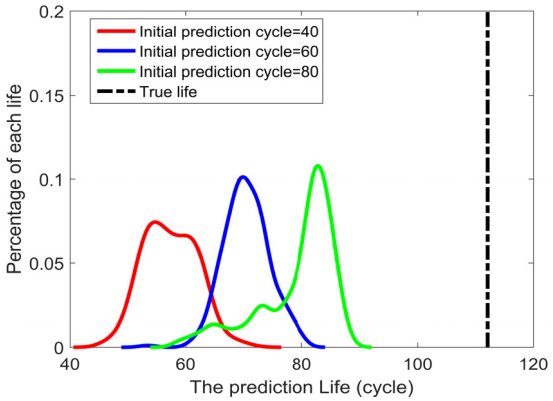

FIGURE 13. RUL probability density distribution based on $V_{CE(on)}$ PF.

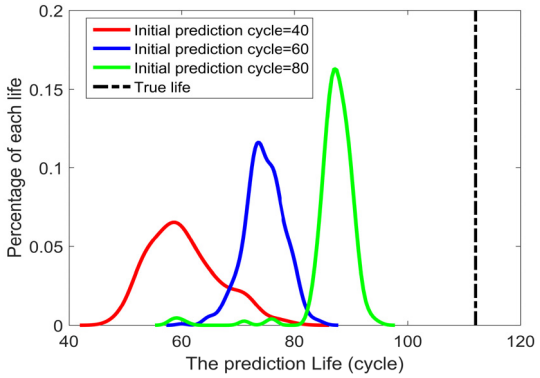

FIGURE 14. RUL probability density distribution based on $V'(V_{CE(on)}, T_j)$ P.F.

TABLE 2. %Error in $V_{CE(on)}$ PF-based RUL estimation with different standard deviation of process noise and measurement noise.

Std.dev of process noise	Std.dev of measurement noise	%error
1e-5	3e-6	13.4%
	3e-5	15.2%
	3e-4	16.1%
1e-4	3e-6	17.0%
	3e-5	13.4%
	3e-4	22.3%
1e-3	3e-6	20.5%
	3e-5	23.2%
	3e-4	25.0%
1e-2	3e-6	26.7%
	3e-5	27.6%
	3e-4	27.6%

The performance of $V_{CE(on)}$ P.F. and $V'(V_{CE(on)}, T_j)$ P.F. is shown in Table 2 and Table 3, respectively, under different process noise and measurement noise when initial prediction cycle is 80. It is observed from Table 2 and

TABLE 3. %Error in $V'(V_{CE(ON)}, T_j)$ PF-based RUL estimation with different standard deviation of process noise and measurement noise.

Std.dev of process noise	Std.dev of measurement noise	%error
1e-5	3e-6	7.1%
	3e-5	7.1%
	3e-4	6.25%
1e-4	3e-6	9.8%
	3e-5	8.9%
	3e-4	8.0%
1e-3	3e-6	15.2%
	3e-5	17.9%
	3e-4	16.7%
1e-2	3e-6	29.4%
	3e-5	31.3%
	3e-4	35.7%

Table 3 that for measurement noise, % error in RUL estimation increases obviously as process noise increases for both methods. In the meanwhile, for process noise, % error in RUL estimation increases slowly as measurement noise increases for both methods as well. Table 3 shows that RUL estimation error can go as low as 6.25% for $V'(V_{CE(on)}, T_j)$ P.F. when standard deviation of measurement process and process noise are less than 3e-4 V and within 1e-5 V. This is evident that $V'(V_{CE(on)}, T_j)$ P.F. performs better than $V_{CE(on)}$ P.F. under different process and measurement noise.

V. CONCLUSION

In this article, a data-driven IGBT RUL prediction method based on particle filter is proposed. This method constructs a new fault precursor $V'(V_{CE(on)}, T_j)$ by fusing T_j and $V_{CE(on)}$ for IGBT condition monitoring. After the preprocessing of the aging data, it shows that the trajectory of $V'(V_{CE(on)}, T_j)$ can be segmented into two regions where region 1 shows linear increasing tendency, while region 2 depicts an exponential increase. The aging model is constructed by piecewise fitting the aging data.

The RUL prediction results show that the proposed fusing parameter P.F. method demonstrates superior performance compared to single P.F. in RUL estimation, and satisfies the rule that the longer the initial prediction period is the smaller the prediction error will be.

REFERENCES

[1] H. Oh, B. Han, P. McCluskey, C. Han, and B. D. Youn, "Physics-of-failure, condition monitoring, and prognostics of insulated gate bipolar transistor modules: A review," *IEEE Trans. Power Electron.*, vol. 30, no. 5, pp. 2413–2426, May 2015, doi: 10.1109/TPEL.2014.2346485.
[2] B. Lu and S. K. Sharma, "A literature review of IGBT fault diagnostic and protection methods for power inverters," *IEEE Trans. Ind. Appl.*, vol. 45, no. 5, pp. 1770–1777, Sep./Oct. 2009, doi: 10.1109/TIA.2009.2027535.

[3] C. Busca, "Modeling lifetime of high power IGBTs in wind power applications–An overview," in *Proc. IEEE Int. Symp. Ind. Electron.*, Jun. 2011, pp. 1408–1413, doi: 10.1109/ISIE.2011.5984366.
[4] B. Gou, X. Feng, W. Song, K. Han, and X. Ge, "Analysis and compensation of beat phenomenon for railway traction drive system fed with fluctuating DC-link voltage," in *Proc. 7th Int. Power Electron. Motion Control Conf.*, Harbin, China, 2012, pp. 654–659, doi: 10.1109/IPEMC.2012.6258823.
[5] B. Ji, V. Pickert, W. Cao, and B. Zahawi, "*in situ* diagnostics and prognostics of wire bonding faults in IGBT modules for electric vehicle drives," *IEEE Trans. Power Electron.*, vol. 28, no. 12, pp. 5568–5577, Dec. 2013, doi: 10.1109/TPEL.2013.2251358.
[6] N. Jiang, M. Chen, S. Xu, W. Lai, G. Bin, and Y. Chen, "Lifetime evaluation of solder layer in an IGBT module under different temperature levels," in *Proc. IEEE 8th Int. Power Electron. Motion Control Conf. (IPEMC-ECCE Asia)*, Hefei, China, 2016, pp. 3137–3141, doi: 10.1109/IPEMC.2016.7512797.
[7] C. Busca, R. Teodorescu, F. Blaabjerg, S. Munk-Nielsen, L. Helle, T. Abeyasekera, and P. Rodríguez, "An overview of the reliability prediction related aspects of high power IGBTs in wind power applications," *Microelectron. Rel.*, vol. 51, nos. 9–11, pp. 1903–1907, 2011.
[8] T. Sreenuch, A. Alghassi, S. Perinpanayagam, and Y. Xie, "Probabilistic Monte-Carlo method for modelling and prediction of electronics component life," *Int. J. Adv. Comput. Sci. Appl.*, vol. 5, no. 1, p. 104, 2014.
[9] M. Ahsan, S. Stoyanov, and C. Bailey, "Data driven prognostics for predicting remaining useful life of IGBT," in *Proc. 39th Int. Spring Seminar Electron. Technol. (ISSE)*, Pilsen, Czech Republic, May 2016, pp. 273–278.
[10] M. Samie, S. Perinpanayagam, A. Alghassi, A. M. S. Motlagh, and E. Kapetanios, "Developing prognostic models using duality principles for DC-to-DC converters," *IEEE Trans. Power Electron.*, vol. 30, no. 5, pp. 2872–2884, May 2015.
[11] A. Alghassi, P. Soulatiantork, M. Samie, S. Perinpanayagam, and M. Faifer, "Reliability enhance powertrain using fuzzy knowledge base prognostics model," in *Proc. 17th Eur. Conf. Power Electron. Appl. (EPE ECCE-Europe)*, Sep. 2015, pp. 1–9.
[12] M. S. Haque, S. Choi, and J. Baek, "Auxiliary particle filtering-based estimation of remaining useful life of IGBT," *IEEE Trans. Ind. Electron.*, vol. 65, no. 3, pp. 2693–2703, Mar. 2018.
[13] M. A. Eleffendi and C. M. Johnson, "In-service diagnostics for wire-bond lift-off and solder fatigue of power semiconductor packages," *IEEE Trans. Power Electron.*, vol. 32, no. 9, pp. 7187–7198, Sep. 2017, doi: 10.1109/TPEL.2016.2628705.
[14] D. W. Brown, M. Abbas, A. Ginart, I. N. Ali, P. W. Kalgren, and G. J. Vachtsevanos, "Turn-off time as an early indicator of insulated gate bipolar transistor latch-up," *IEEE Trans. Power Electron.*, vol. 27, no. 2, pp. 479–489, Feb. 2012, doi: 10.1109/TPEL.2011.2159848.
[15] L. Dupont and Y. Avenas, "Preliminary evaluation of thermo-sensitive electrical parameters based on the forward voltage for online chip temperature measurements of IGBT devices," *IEEE Trans. Ind. Appl.*, vol. 51, no. 6, pp. 4688–4698, Nov. 2015, doi: 10.1109/TIA.2015.2458973.
[16] J. Han, M. Ma, K. Chu, X. Zhang, and Z. Lin, "*In-situ* diagnostics and prognostics of wire bonding faults in IGBT modules of three-level neutral-point-clamped inverters," in *Proc. IEEE 8th Int. Power Electron. Motion Control Conf. (IPEMC-ECCE Asia)*, Hefei, China, May 2016, pp. 3262–3267.
[17] K. Chu "Research on *in-situ* monitoring of wire bonding faults in IGBT modules based on multi-dimensional data model," (in Chinese), M.S. thesis, Hefei Univ. Technol., Hefei, China, 2018.
[18] T. K. Gachovska, B. Tian, J. Hudgins, W. Qiao, and J. F. Donlon, "A real-time thermal model for monitoring of power semiconductor devices," *IEEE Trans. Ind. Appl.*, vol. 51, no. 4, pp. 3361–3367, Jul./Aug. 2015.
[19] W. He, N. Williard, M. Osterman, and M. Pecht, "Remaining useful performance analysis of batteries," in *Proc. IEEE Conf. Prognostics Health Manage.*, Montreal, QC, Canada, 2011, pp. 1–6.
[20] W. He, N. Williard, M. Osterman, and M. Pecht, "Remaining useful performance analysis of batteries," in *Proc. IEEE Conf. Prognostics Health Manage.*, Montreal, QC, Canada, Jun. 2011, pp. 1–6.
[21] S. Cheng and J. Zhang, "Particle filter review," (in Chinese), *J. Astronaut.*, vol. 4, pp. 1099–1111, Apr. 2008.

ZHEN RAO was born in Fuzhou, Jiangxi, China, in 1997. She received the bachelor's degree in electrical engineering from Nanjing Normal University, Nanjing, China, in 2018. She is currently pursuing the master's degree. Her main research interest includes reliability of power electronic devices.

MENG HUANG (Member, IEEE) received the B.Eng. and M.Eng. degrees from the Huazhong University of Science and Technology, Wuhan, China, in 2006 and 2008, respectively, and the Ph.D. degree from The Hong Kong Polytechnic University, Hong Kong, in 2013. He is currently an Associate Professor with the School of Electrical Engineering, Wuhan University, Wuhan. His research interests include non-linear analysis of power converters and power electronics reliability.

XIAOMING ZHA (Member, IEEE) was born in Huaining, Anhui, China, in 1967. He received the B.S., M.S., and Ph.D. degrees in electrical engineering from Wuhan University, Wuhan, China, in 1989, 1992, and 2001, respectively. He was a Postdoctoral Fellow with the University of Alberta, Canada, from 2001 to 2003. He has been a Faculty Member with Wuhan University, since 1992, where he became a Professor, in 2003. He is currently the Deputy Dean of the School of Electrical Engineering, Wuhan University. His research interests include power electronic converter, the application of power electronics in smart grid and renewable energy generation, the analysis and control of microgrid, the analysis and control of power quality, and frequency control of high-voltage high-power electric motors.